Physica B 643 (2022) 414180

Contents lists available at ScienceDirect

Physica B: Physics of Condensed Matter

journal homepage: www.elsevier.com/locate/physb

Thermodynamic properties of perturbed monolayer PbBiI

Nguyen N. Hieu [a,b], Chuong V. Nguyen [c], Huynh V. Phuc [d], Bui D. Hoi [e,f,*], Tran C. Phong [f,*]

[a] Institute of Research and Development, Duy Tan University, Danang 550000, Viet Nam
[b] Faculty of Natural Sciences, Duy Tan University, Danang 550000, Viet Nam
[c] Department of Materials Science and Engineering, Le Quy Don Technical University, Ha Noi, Viet Nam
[d] Division of Theoretical Physics, Dong Thap University, Cao Lanh 870000, Viet Nam
[e] Department of Physics, University of Education, Hue University, Hue 530000, Viet Nam
[f] Center for Theoretical and Computational Physics, University of Education, Hue University, Hue 530000, Viet Nam

ARTICLE INFO

Keywords:
Thermodynamic properties
Green's function approach
Noncentrosymmetric quantum spin Hall insulators
PbBiI monolayer
Perturbation

ABSTRACT

In this paper, we theoretically investigate the influence of external electric field, Zeeman splitting field, and dilute charged impurity on the thermodynamic features of the PbBiI monolayer. Green's function approach, the Born approximation, and the tight-binding model are employed to address these effects. We find the responses of the electronic heat capacity (HC) and Pauli spin paramagnetic susceptibility (PSPS) to the symmetry breaking originated from the presence of the perturbations. The results show that the electric (Zeeman) field leads to an increase (decrease) in the bulk gap of the system, resulting in a gapless phase at a critical Zeeman field. Correspondingly, HC and PSPS results confirm almost zero responses at the appeared critical Zeeman field. On the other hand, critical impurity characters emerge within the validity regime of the Born approximation. Finally, the combined effects of these perturbations are compared with the findings from the individual ones.

1. Introduction

It is well-established that two-dimensional (2D) topological insulators (TIs) provide a promising platform for spintronics and topological quantum computing [1–3]. 2D TIs with non-trivial band gaps usually contain heavy elements with strong intrinsic spin–orbit coupling (SOC) [4–10]. In addition to the intrinsic SOC, the parallel spin-polarized band dispersion curves accompanied by the opposite in-plane chiral spin texture due to lack of inversion symmetry can be regarded as an extrinsic SOC, so-called Rashba effect [2,11,12]. This extrinsic SOC produces an effective electric field, which allows the control of the spin direction in the system [13–19]. Quantum spin Hall insulators (QSHIs) [1] regarded as 2D TIs support topologically protected helical metallic edge states and maintain an insulating bulk [20].

PbBiI compound as an example of noncentrosymmetric honeycomb-lattice QSHIs has already been introduced to the literature with a Rashba potential of 60 meV and band inversion with a large nontrivial band gap of 0.14 eV in the work of Acosta and co-workers [21]. More importantly, it has been shown that a Rashba-like spin splitting is formed in the PbBiI compound by two bands with the same in-plane helical spin texture. These results allow the potential application of such materials in the spintronic device with less energy loss. In another work [22], it has been demonstrated that a Zeeman-type spin splitting can be formed in noncentrosymmetric 3D compounds. This splitting can be tuned by changing the growth direction of slabs in these compounds. Many of the above results are thought to occur because the systems have certain excitations of the states hosting the electrons. Further, the coexistence of the ferroelectric and valley polarization in 2D robust TIs, a family of fluorinated methyl-functionalized bismuthene ($Bi_2C_2H_{6-x}F_x$) films with strong SOC (resulting in a non-trivial band gaps up to 1.08 eV), has been studied [23]. Based on first-principles calculations [24], the methyl-functionalized InBi monolayer ($InBiCH_3$) has QSH-state hosts with a band gap as large as 0.29 eV, which is tunable and robust against the external electromechanical fields. Generally, high structural stability and large-gap in 2D III–V films promise the potential application of them [25–29].

There are many researches focused on the physical properties of such systems, however, on noncentrosymmetric 2D QSHIs, the systematic inclusion of perturbation effects has yet to be attempted for any of these systems. Massive investments in designing new materials for next-generation electronic and magnetic devices are opening a new chapter in quantum materials, the investigation of emergent electronic, thermodynamic and thermal properties [30–35]. These features will propose some information that may be useful alongside solar cells and catalysts as targets of absolute priority for designer materials intended for technological application. In this work, we particularly investigate

* Corresponding authors.
E-mail addresses: buidinhhoi@hueuni.edu.vn (B.D. Hoi), tcphong.sp@hueuni.edu.vn (T.C. Phong).

https://doi.org/10.1016/j.physb.2022.414180
Received 22 April 2022; Received in revised form 28 June 2022; Accepted 5 July 2022
Available online 8 July 2022

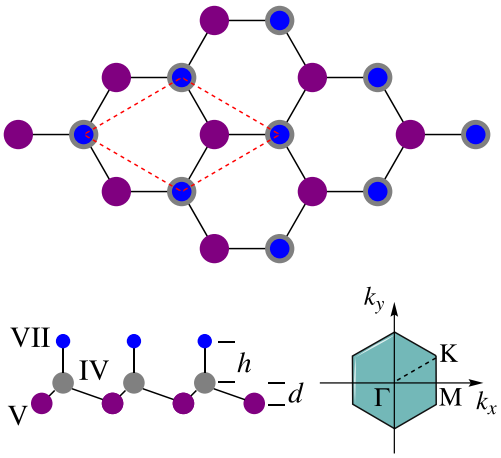

Fig. 1. Real-space top and side views of a noncentrosymmetric honeycomb-lattice QSHI, formed by the IV, V, and VII elements, associated with the buckling parameter $d = 1.3$ Å and the bond lengths $\{h = 1.35, 3.04\}$ Å for {Bi-Pb, Pb-I}. The $k_y - k_x$ plane shows the reciprocal space.

unconventional "perturbed" electronic and thermodynamic properties of stable, noncentrosymmetric honeycomb-lattice QSHIs, formed by the IV, V, and VII elements. The perturbations are the electric field, the Zeeman magnetic field, and the dilute charged impurities. To do so, we focus on the fundamental electronic band structure, electronic heat capacity (HC) and the Pauli spin paramagnetic susceptibility (PSPS) based on the tight-binding model, the Green's function calculations and the Born approximation in the scattering theory [36,37].

This paper is structured as follows. In Section 2, we briefly show the necessary tight-binding Hamiltonian model, the HC, and the PSPS in a pristine (unperturbed) QSHI. Section 3 presents the results for the effects of the above-mentioned perturbations on the electronic band structure, HC, and PSPS. Finally, concluding remarks will be presented in Section 4.

2. Pristine QSHIs of PbBiI compound

We introduce a model of a QSHI made up of elements of groups IV, V and VII, such as the PbBiI compound as illustrated in Fig. 1 and previously described in detail in Ref. [38]. In Fig. 1, the QSHI structure has a buckled honeycomb form with two sublattices A and B (elements of group V) and a dimer (IV–VII elements). It has been shown in Ref. [21] that the orbital contribution of Pb-I dimers near the Fermi level is smaller than that of Bi atoms and can be neglected. Using the basis of SOC of the Bi atoms$|\mathrm{Bi}_{J,J_z}\rangle$, one can write the effective Hamiltonian matrix in the compound PbBiI, as a typical QSHI, as follows

$$\mathcal{H}(\vec{k}) = \begin{pmatrix} -\varepsilon_{1/2} + \zeta_{1/2}k^2 & \mathrm{i}\alpha_{R1}^{1/2}[k_x - \mathrm{i}k_y] & 0 & \gamma[k_x - \mathrm{i}k_y] \\ -\mathrm{i}\alpha_{R1}^{1/2}[k_x + \mathrm{i}k_y] & -\varepsilon_{1/2} + \zeta_{1/2}k^2 & \gamma[k_x + \mathrm{i}k_y] & 0 \\ 0 & \gamma[k_x + \mathrm{i}k_y] & +\varepsilon_{3/2} - \zeta_{3/2}k^2 & 0 \\ \gamma[k_x - \mathrm{i}k_y] & 0 & 0 & +\varepsilon_{3/2} - \zeta_{3/2}k^2 \end{pmatrix}, \tag{1}$$

where on-site energies of different angular momenta are given by the diagonal constant energies [$\varepsilon_{1/2} = 0.1685$ eV, $\varepsilon_{3/2} = 0.1575$ eV, $\alpha_{R1}^{1/2} = 3.0919$ eV/Å, $\zeta_{1/2} = 0.008187$ eV/Å^2, $\zeta_{3/2} = 0.038068$ eV/Å^2] [21], while the next-nearest-neighbor hopping processes are described by off-diagonal ones. Also, $\vec{k} = (k_x, k_y)$ is the momenta in the first Brillouin zone (FBZ). And, $\gamma = -3.5853$ eV/Å. The energy dispersion relation corresponding to the Hamiltonian (1) is obtained as [38]

$$\mathcal{E}_\tau^\sigma(k) = \frac{1}{2}\left[\sigma\alpha_{R1}^{1/2}k + \varepsilon + \zeta k^2 + \tau\left\{\left(4\gamma^2 + \left[\alpha_{R1}^{1/2}\right]^2\right)k^2 + \left[\varepsilon' - \zeta' k^2\right]\left[-2\sigma\alpha_{R1}^{1/2}k + \varepsilon' - \zeta' k^2\right]\right\}^{1/2}\right], \tag{2a}$$

$$\varepsilon := \varepsilon_{3/2} - \varepsilon_{1/2} \quad , \quad \varepsilon' := \varepsilon_{3/2} + \varepsilon_{1/2} \quad ,$$

$$\zeta := \zeta_{1/2} - \zeta_{3/2} \quad , \quad \zeta' := \zeta_{1/2} + \zeta_{3/2}\,. \tag{2b}$$

where $\tau = +1$ (-1) for the conduction (valence) band and $\sigma = +1$ (-1) implies the spin up (down).

In Fig. 2(a), we plot the electronic band structure of the pristine PbBiI structure. One can see the existence of two different energy gaps at the Γ point: the Rashba spin splitting ($\mathcal{E}_R \simeq 60$ meV) gap and the band inversion gap ($\mathcal{E}_{g\Gamma} \simeq 250$ meV). It has been shown in Ref. [21] that the energy $\mathcal{E}_R$ can be increased up to 90 meV via a compressive strain. The highest valence band is mainly originated from the $p_{x,y}$-Bi orbitals, while the lowest conduction band is mainly formed by p_z-Bi orbitals.

Now we turn to the main purpose of the present work, which is to study the HC and PSPS of PbBiI compound. The HC as a thermodynamic quantity that is directly related to the electronic properties of the material [39]. However, here we only consider the contribution of electrons to the HC, the contribution of phonons will be of interest in our future works. In general, HC is the change of the total internal energy of N electrons per unit change of temperature, i.e. $C^0(T) = d\,\mathcal{U}^0/dT$ where $\mathcal{U}^0$ is the total internal energy given by

$$\mathcal{U}^0 = \int_{-\infty}^{\infty} d\mathcal{E}\,\mathcal{E}\,n_{\mathrm{FD}}(\mathcal{E},T)\,\mathcal{D}^0(\mathcal{E})\,, \tag{3a}$$

in which $n_{\mathrm{FD}}(\mathcal{E},T)$ is the Fermi–Dirac distribution function of electrons with energy $\mathcal{E}$ at temperature T. Also, $\mathcal{D}^0(\mathcal{E})$ denotes the electron density of states (DOS) in the pristine (unperturbed) system. Thus, we have

$$\begin{aligned} C^0(T) &= \int_{-\infty}^{+\infty} d\mathcal{E}\,\mathcal{E}\left(\frac{\partial n_{\mathrm{FD}}(\mathcal{E},T)}{\partial T}\right)\mathcal{D}^0(\mathcal{E}) \\ &= \frac{1}{2k_{\mathrm{B}}T^2}\int_{-\infty}^{+\infty} d\mathcal{E}\,\frac{\mathcal{E}^2}{1+\cosh\left[\mathcal{E}/k_{\mathrm{B}}T\right]}\,\mathcal{D}^0(\mathcal{E})\,, \end{aligned} \tag{4}$$

where k_{B} is the Boltzmann constant and we have set $\mathcal{E}_{\mathrm{F}} = 0$. The electronic DOS can be connected to the Hamiltonian in Eq. (1) using the Green's function via $\mathcal{D}^0(\mathcal{E}) = -(1/2\pi)\sum_{\vec{k}\in\mathrm{FBZ}}\sum_{\alpha=1}^{4}\mathrm{Im}[G^0_{\alpha\alpha}(\vec{k},\mathcal{E})]$ where the unperturbed Green's function matrix is given by [36,37]

$$G^0(\vec{k},\mathcal{E}) = \left[\mathcal{E} + \mathrm{i}\eta - \mathcal{H}(\vec{k})\right]^{-1}, \tag{5}$$

where $\eta = 5$ meV is the phenomenological infinitesimal broadening factor. The evolution of the HC with temperature is demonstrated in Fig. 2(b) (the blue curve). We can see clearly the appearance of the Schottky anomaly in the HC at $k_{\mathrm{B}}T \simeq \mathcal{E}_{g\Gamma}$ as expected. The origin and physical meaning of this anomaly can be understood clearly as analyzed in a previous work for borophene monolayer [40].

Turning to another thermodynamic property, so-called PSPS, which is well suited for classifying solid materials based on their magnetic properties. Magnetic materials exhibit an internal magnetization $(\mathcal{M})$ when being subjected to an external magnetic field (H). The magnetic susceptibility (χ), on the other hand, is defined as the ratio of this magnetization to the magnetic field strength. From these points, depending on the behavior of the material with the applied magnetic field, the responses are classified into three main groups including antiferromagnetic (AFM), paramagnetic (PM) and ferromagnetic (FM). In general, the magnetic susceptibility can be calculated via the DOS. The formula for the magnetization density is [36,37]

$$\mathcal{M} = \frac{\mu_{\mathrm{B}}}{2}\int_{-\infty}^{\infty}\mathcal{D}^0(\mathcal{E})d\mathcal{E}\left[n_{\mathrm{FD}}(\mathcal{E}-\mu_{\mathrm{B}}H) - n_{\mathrm{FD}}(\mathcal{E}+\mu_{\mathrm{B}}H)\right], \tag{6}$$

where μ_{B} is the Bohr magneton. Expanding the Fermi distribution with respect to the magnetic field and ignoring terms containing higher powers of the magnetic field when the magnetic field is weak $(H \to 0)$, we have

$$\mathcal{M} = \mu_{\mathrm{B}}^2 H\int_{-\infty}^{\infty}\mathcal{D}^0(\mathcal{E})\frac{-\partial n_{\mathrm{FD}}(\mathcal{E},T)}{\partial\mathcal{E}}d\mathcal{E}, \tag{7}$$

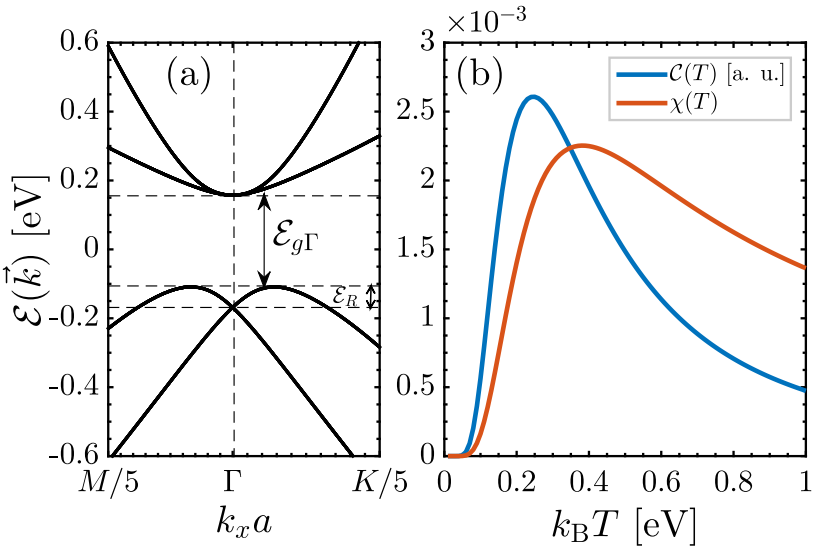

Fig. 2. (a) Electronic band structure, (b) HC and PSPS of non-interacting PbBiI in the absence of perturbations. The energy $\mathcal{E}_{g\Gamma} \simeq 250$ meV and $\mathcal{E}_R \simeq 60$ meV refers to the band inversion gap and the Rashba spin splitting, respectively. (For interpretation of the references to color in this figure legend, the reader is referred to the web version of this article.)

from that the PSPS is written as

$$\chi(T) = \mu_B^2 \int_{-\infty}^{\infty} D^0(\mathcal{E})[-\partial_{\mathcal{E}} n_{\rm FD}(\mathcal{E}, T)] d\mathcal{E}. \tag{8}$$

Similar to the HC, it is appropriate to briefly review PSPS in magnetic materials, particularly AFM ones. It has been shown that there are two or more sublattices that are magnetized in opposite directions in AFM materials. AFM materials turn to PM ones at the temperature above a critical temperature, the Neel temperature, which is obtained from the maximum of the susceptibility. The value of PSPS reaches maximum at $T = T_N$ and then decreases with increasing T. The red curve in Fig. 2(b) presents the unperturbed PSPS of the PbBiI compound versus thermal energy. We can see that the PSPS curve first increases, reaches a maximum value, and then decreases. The physical reason behind a different position of the peak in $\chi(T)$ compared to HC backs to the energy derivative of the Fermi–Dirac distribution function, see Eq. (8). In contrast to HC, PSPS is more sensitive to the concavity of bands because of the energy derivative process. For this reason, the position of the peak T_N appears at higher thermal energies than $\mathcal{E}_{g\Gamma}$.

3. Perturbation effects on the HC and PSPS of PbBiI compound

3.1. Electric and Zeeman fields

After addressing the basic electronic and thermodynamic features of the pristine PbBiI compound, we turn to the perturbation effects. We start with the electric and Zeeman field effects on the electronic phase of the PbBiI compound via the following models

$$\hat{\mathcal{H}}^{\sigma}_{\rm buck.} = -\sum_i \frac{\sigma V}{2} \hat{f}^{\dagger}_{i\sigma} \hat{f}_{i\sigma}, \tag{9a}$$

$$\hat{\mathcal{H}}_{\rm Zeeman} = \frac{g\mu_B \mathcal{B}}{2} \sum_{i,j} \left[\hat{f}^{\dagger}_{i\uparrow} \hat{f}_{i\downarrow} + \hat{f}^{\dagger}_{i\uparrow} \hat{f}_{j\downarrow} + \text{H.c.} \right], \tag{9b}$$

where $V = eEd$, e is the electron charge, E is the strength of applied electric field, and $d = 1.3$ Åis the sublattice separation. We stress that the considered electric field is uniform with different signs for different spins originating from the buckling of the system. The summations are taken for all lattice sites between i and j. The creation and annihilation operator for an electron with spin σ at site i and j, respectively, is described by $\hat{f}^{\dagger}_{i\sigma}$ ($\hat{f}_{j\sigma}$). On the other hand, g is the degeneracy number, μ_B is the Bohr magneton, and $\mathcal{B}$ is the Zeeman magnetic field strength. Finally, the term H.c. denotes the Hermitian conjugate of operators.

With the help of the Fourier transformation, the total Hamiltonian in the presence of electric and magnetic fields can be rewritten as given in Box I.

Again, one can calculate the electric- and Zeeman field-induced energy dispersion by diagonalizing the above Hamiltonian. Also, the electronic DOS of the system in the presence of electric and magnetic fields can be calculated through $G(\vec{k}, \mathcal{E}) = [\mathcal{E} + i\eta - \mathcal{H}_{\rm per}(\vec{k})]^{-1}$. As well-known, the corresponding results for HC and PSPS can also be found. To focus on the main aim of the present paper, we only consider one strength of the electric and Zeeman field to address the electronic band structure of the PbBiI compound.

First we set $\mathcal{B} = 0$. In Fig. 3(a) the band structures for a model with $V = 1$ eV is shown. We immediately point out that the C_{3v} symmetry [21], comprising of threefold rotation symmetry R_3 along the z axis, mirror symmetry M_x ($x \to -x$) in the yz plane, and (iii) TR symmetry $\mathcal{T}$, is broken with the electric field and the position of the band gaps introduced before is changed with V. This symmetry breaking is removing the Rashba gap explicitly and the intersection points (the saddle points corresponding to the gap at Γ point) such that both gaps form a new gap at the Γ point. The band separation may lead to the new degenerate states in the system because the bands are getting flat with V. These effects will also manifest themselves in the perturbed HC and PSPS.

Further, Fig. 3(b) shows the behavior of the band structure with the Zeeman splitting field. Again the C_{3v} symmetry breaking occurs. In contrast to the electric field, the changes with the Zeeman field are not symmetric with respect to the K and M points in the FBZ. Like before, the inherent gaps are disappeared with the Zeeman field and bands start to cross each other due to the splitting effect. Here we set $g\mu_B\mathcal{B} = 0.7$ eV to see the crossing point of the bands at the Fermi level. Again, we will observe the effect of band splitting due to the Zeeman field on the HC and PSPS quantities.

In Fig. 4 and the following figures, we will use the general procedure outlined before in order to capture the electric and Zeeman field effects on the HC and PSPS of the PbBiI compound. For DOS details, one can be referred to the Ref. [38]. Shown in Figs. 4(a) and 4(b) are respectively $C(T)$ and $\chi(T)$ for three different Vs compared to the pristine situation, i.e. $V = 0$. We set the Zeeman field to zero to see the sole role of the electric field on the Schottky anomaly. All strengths show the same treatment described before, increasing and decreasing behaviors after the Schottky temperature with V. However, the HC increases with V stemming from the fact that the band gap increases with the

$$\mathcal{H}_{\rm per}(\vec{k}) = \begin{pmatrix} -\varepsilon_{1/2} + \zeta_{1/2}k^2 - V/2 & \mathrm{i}\alpha_{\rm R1}^{1/2}k_- + g\mu_{\rm B}\mathcal{B}/2 & 0 & \gamma k_- + g\mu_{\rm B}\mathcal{B}/2 \\ -\mathrm{i}\alpha_{\rm R1}^{1/2}k_+ - g\mu_{\rm B}\mathcal{B}/2 & -\varepsilon_{1/2} + \zeta_{1/2}k^2 + V/2 & \gamma k_+ - g\mu_{\rm B}\mathcal{B}/2 & 0 \\ 0 & \gamma k_- + g\mu_{\rm B}\mathcal{B}/2 & \varepsilon_{3/2} - \zeta_{3/2}k^2 - V/2 & g\mu_{\rm B}\mathcal{B}/2 \\ \gamma k_+ - g\mu_{\rm B}\mathcal{B}/2 & 0 & -g\mu_{\rm B}\mathcal{B}/2 & \varepsilon_{3/2} - \zeta_{3/2}k^2 + V/2 \end{pmatrix}. \quad (10)$$

Box I.

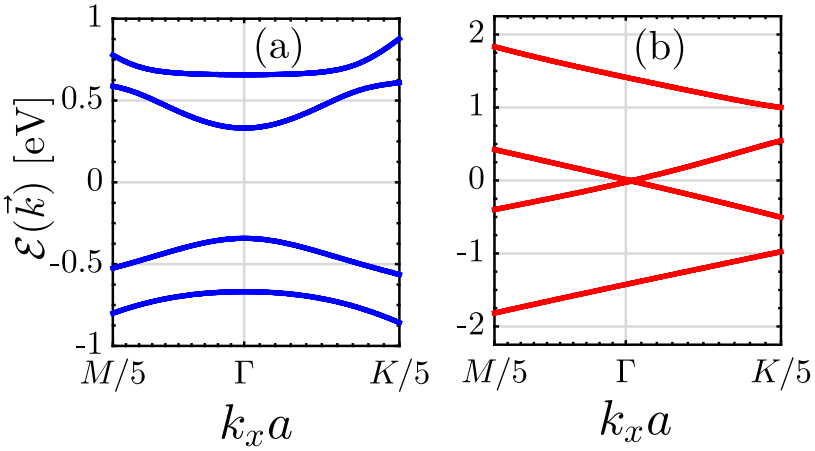

Fig. 3. Electronic band structure of PbBiI compound at (a) $V = 1.0$ eV and (b) $g\mu_{\rm B}\mathcal{B} = 0.7$ eV.

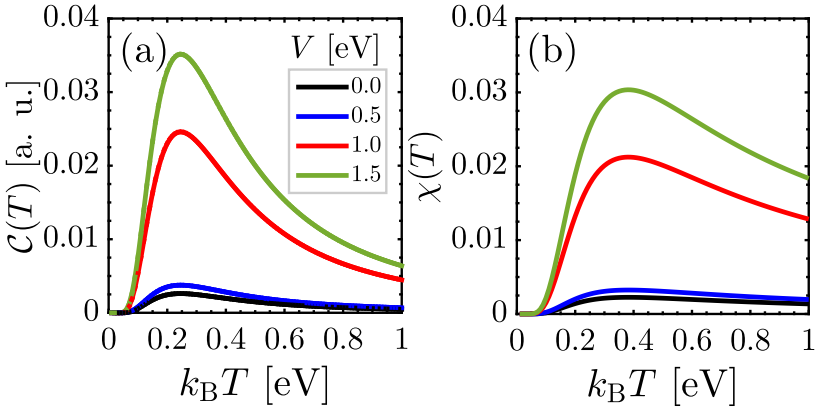

Fig. 4. The evolution of (a) HC and (b) PSPS of PbBiI compound with the electric field when the Zeeman field is turned off.

electric field as soon as the C_{3v} symmetry is broken. One may expect some changes in the Schottky position, but it should be noted that the Schottky peak shown in Fig. 2(b) corresponding to the bulk gap of the system will not follow the gap anymore when the C_{3v} symmetry starts to break down. For this reason, this symmetry breaking leads to an increase in the HC, and no change is observed for the Schottky position with V. The same argument is valid for the PSPS peak and its behavior with the electric field. By this, we mean that PSPS increases with V in Fig. 4(b) along with no change in the peak position, see above.

In contrast to the electric field, an interesting behavior originated from the closed band gap in Fig. 3(b) appears for both quantities. We learned that a critical Zeeman field results in a gapless phase in the system associated with the C_{3v} symmetry breaking. Due to the highly connected electronic and thermodynamic features, this gapless phase manifests itself in both HC and PSPS such that they increase with Zeeman field up to a critical value and then start to immediately decrease belonging to the gapless phase. For this reason, at $g\mu_{\rm B}\mathcal{B} = 0.7$ eV, both HC and PSPS quantities approach zero compared to other strengths. However, these results can be modulated in the presence of other perturbations; we will come to this point in Fig. 7.

There are two important points about the formed curves in both Figs. 4 and 5 at intermediate temperatures in the presence of strong V and critical $g\mu_{\rm B}\mathcal{B}$ as general principles. First is the relation $\chi(T) < C(T)$, which is valid in the absence and presence of local perturbations stemming from the occupation number multiplied by the fermion energy [see Eq. (4)]. The second point immediately refers to the small intensities of quantities in the presence of the Zeeman field compared to the ones with the electric field, meaning that the responses with the Zeeman field are dealing with fewer states. This can be understood from the fact that degeneracy states in the electronic DOS of the system subjected to the Zeeman field are less than that of the electric field-induced one, see Fig. 3.

3.2. Dilute charged impurity

We now investigate the effect of dilute charged impurity on the DOS, and followed by the HC and PSPS of the system. This perturbation

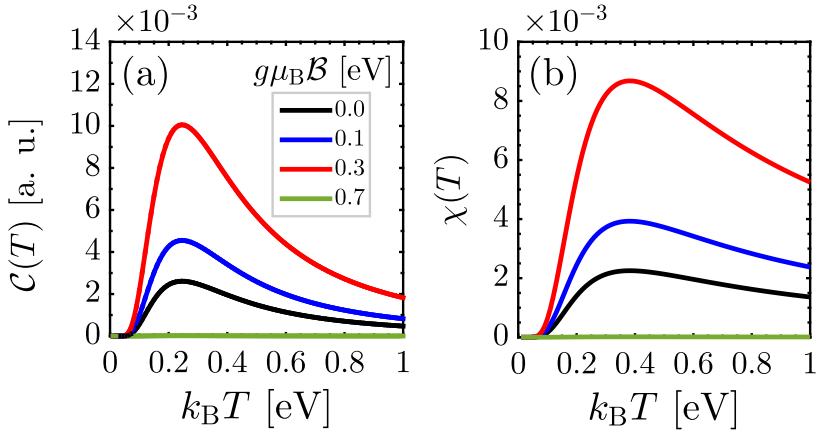

Fig. 5. The evolution of (a) HC and (b) PSPS of PbBiI compound with Zeeman field when the electric field is turned off.

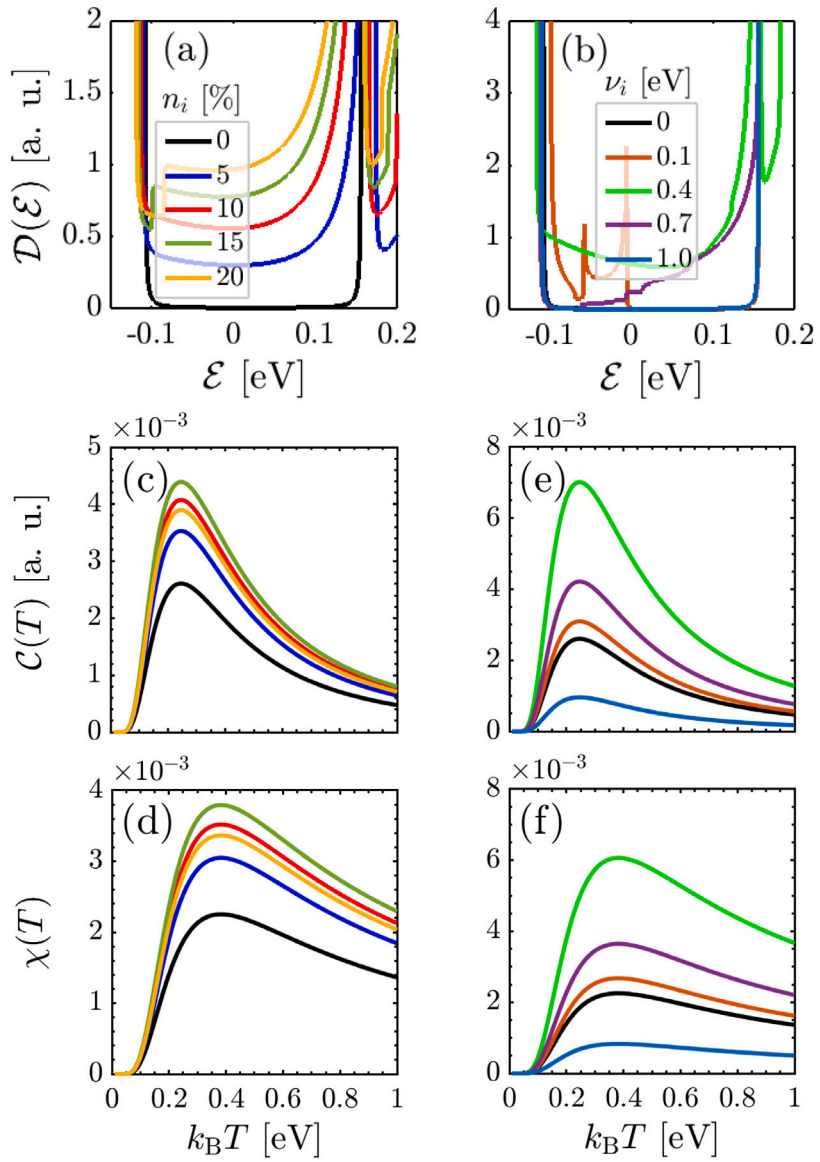

Fig. 6. The *perturbed* electronic DOS of *impurity-infected* PbBiI compound when (a) the scattering potential is fixed at $\nu_i = 0.5$ eV and (b) the impurity concentration is fixed at $n_i = 10\%$. The electric and magnetic fields are switched off in this plot. The corresponding HC and PSPS are represented in {(c),(d)} and {(e),(f)}, respectively.

can be described through the interacting Hamiltonian of the electrons and external impurities which has been presented in Ref. [38] as

$$\hat{\mathcal{H}}_{\text{e-i}} = \sum_{\vec{k},\vec{q}} v_{\text{i}} \hat{f}^{\dagger}_{\vec{k}+\vec{q}} \hat{f}_{\vec{q}} \quad , \quad \hat{f} := \text{unit cell atoms}\,, \tag{11}$$

where $\vec{q} = (q_x, q_y)$. We consider dilute charged impurities distributed randomly in the system with the impurity concentration $n_i = N_i/V$ [N_i is the number of impurities and V is the volume of numerically implemented unit cells] and scattering potential v_i. The perturbed Green's function is given by [36,37]

$$\hat{G}(\vec{q},\tau) = -\langle T_\tau U(\beta,0) \hat{f}_{\vec{q}}(\tau) \hat{f}^{\dagger}_{\vec{q}}(0)\rangle_0\,, \tag{12}$$

where $\beta = 1/k_{\text{B}}T$, τ is the imaginary time, and $U(\beta,0)$ is the time evolution operator given by

$$U(\beta,0) = T\, e^{-\text{i}\int_0^\beta \mathcal{H}_{\text{e-i}}(\tau)\, d\tau}\,. \tag{13}$$

To neglect the effect of phonons, we limit ourselves to the low impurity density, then the electronic self-energy matrix elements of disordered PbBiI lattice can be calculated utilizing the Born approximation and T-matrix [36,37] as

$$\Sigma(\vec{q},\mathcal{E}) = n_i v_i \Big[1 - \frac{v_i}{N_{\text{a}}} \sum_{\vec{k}\in\text{FBZ}} G_0(\vec{k},\mathcal{E})\Big]^{-1}\,. \tag{14}$$

Using the Dyson equation [36], one can expand the perturbed Green's function of the impurity-infected QHSI as

$$G(\vec{k},\mathcal{E}) = G_0(\vec{k},\mathcal{E}) + G_0(\vec{k},\mathcal{E})\Sigma(\vec{q},\mathcal{E})G(\vec{k},\mathcal{E})\,. \tag{15}$$

The *perturbed* DOS now can be obtained from the trace over the imaginary part of the retarded *interacting* Green's function

$$D(\mathcal{E}) = -\frac{1}{\pi N_a} \sum_{\chi=1}^{4} \sum_{\vec{k}\in\text{FBZ}} \text{Im}\Big[G^{\chi\chi}(\vec{k},\mathcal{E})\Big]\,. \tag{16}$$

In the following, we numerically investigate the DOS, HC and PSPS of the PbBiI compound for two scenarios: (i) the same impurity atoms ($v_i = constant$) and different n_i and (ii) different impurity atoms (v_i varies) and the same n_i. The electronic DOS is shown in Figs. 6(a) and 6(b) for the former and the latter, respectively, where we fix the scattering potential v_i at 0.5 eV (Fig. 6(a)) and the impurity concentration n_i at 10% (Fig. 6(b)). The detailed analyzes for the DOS for both the scenarios have been presented clearly in Ref. [38] which investigated the electronic phases in the PbBiI QSHI. In this work, we focus only on the HC and PSPS of the system under the charged impurity perturbation.

Having the electronic DOS, one immediately turns to the HC and PSPS through Eqs. (4) and (8). Fig. 6(c)–(f) denote the numerical results. Strong deviations from the linearly increased trends with both impurity scattering parameters n_i and v_i addressed by the invalidity of the Born approximation are evident. Looking at Fig. 6(a), we observe that the new mid-gap degenerate states start to appear (characterized by the singularity around $\mathcal{E} \simeq -0.09$ eV at $n_i \simeq 15\%$) for which the DOS is strongly increased and above this concentration $n_i \simeq 15\%$, the system tends to take stronger degenerate states, leading to larger DOSs at other energies. This, in turn, manifest itself in the HC and PSPS since the DOS is directly included in Eqs. (4) and (8). When the DOS is large, the HC and PSPS become large as well. However, for $n_i = 20\%$, the density of states around the singularity is close to the case of $n_i = 10\%$ and for this reason, the competition between energies in HC and PSPS leads to similar smaller responses. On the other hand, in Fig. 6(b), the system transits from partially zero DOS to fully non-zero DOS at $v_i \simeq 0.4$ eV. For the same reason above-mentioned for the relation between DOS and HC/PSPS, both HC and PSPS become large at this impurity potential. It should be pointed out that intensities obtained here for both scenarios are in the same order, which is another confirmation to the theory we applied because both scattering parameters are originated from the first-order perturbation theory and they both belong to the randomly doped impurities. For this reason, it is not far from the fact that close intensities are expected to emerge. Like before, all these arguments may be changed if other perturbations are involved in the scattering process.

As the last investigation, we turn to the combined effects of perturbations. Although there are many possibilities to this end, we fix the impurity scattering parameters to $n_i = 10\%$ and $v_i = 0.5$ eV and focus on the alterations of HC and PSPS with both electric and Zeeman fields in Fig. 7. Remarkably, there is no nontrivial response for HC and PSPS with V when the charged impurity is present. This stems from the point that both electric field and charged impurity doping disturbances are types of electronic perturbations and the electric field is robust against the *dilute* impurity doping. This may not be the case if dense impurities are doped randomly on the system, which requires other approximations and it is out of the scope of the present paper. In more detail, as presented in the electronic DOSs in Fig. 6, the impurity concentration and scattering potential cannot take larger values than those taken — the system does not respond anymore for $v_i > 1$ eV and $n_i > 20\%$ because the DOSs are going back to their initial trends. This argument is evident for $v_i > 1$ eV, while for $n_i > 20\%$, this means that the singularities move to the conduction band and the DOS becomes similar to the pristine case. This is the way we characterize the invalidity of Born approximation which is valid only for dilute impurities. Looking at the intensities in Figs. 7(a) and 7(b), we notice that the general statement $\chi(T) < C(T)$ is not valid anymore in the presence of impurity and one should report it in another way. However, they are still so close to each other. Here there is a *screening effect* at which doping induces screening potential to the atoms, resulting in the reduction of carrier's energy and eventually in reducing the HC compared to the PSPS.

Although there is a nontrivial response at $g\mu_{\text{B}}\mathcal{B} = 0.3$ and 0.7 eV (the same unexpected responses — accidentally due to the energy scale competitions in the corresponding DOSs and bandwidths of the electronic band structure) for both HC and PSPS to the Zeeman field combined with the impurity doping, as shown in Figs. 7(c) and 7(d), which was not the case in the absence of impurity doping in Fig. 5, for the Zeeman field, one should think of another mechanism because Zeeman field and dilute charged impurity are types of different electronic and magnetic perturbations. Thus, the screening effect mentioned before is not affecting the Zeeman field effects. By this, we mean that the relation $\chi(T) < C(T)$ holds valid when the Zeeman field coexists with the dilute impurity doping.

4. Concluding remarks

To summarize, we have carried out a theoretical study of the thermodynamic properties of noncentrosymmetric QSHIs, to capture the electric field, Zeeman field, and dilute charged impurity scattering effects on electronic HC and PSPS of PbBiI compound as an alternating noncentrosymmetric QSHI. We have employed Green's function technique to find the electronic DOS, the semi-classical Boltzmann approach to find HC and PSPS, the tight-binding Hamiltonian model to consider the electric and Zeeman fields, and the Born approximation to include the dilute charged impurity doping effects.

Three kinds of behaviors are being involved as soon as the C_{3v} symmetry is broken under perturbations: (i) increase of the bulk band gap, HC and PSPS with the electric field without any nontrivial treatment, (ii) decrease of the bulk band gap, HC and PSPS with the Zeeman magnetic field with a nontrivial gapless phase at a critical field in the band gap and zero responses in both HC and PSPS, and (iii) invalidity of employed Born approximation at a certain critical impurity concentration and scattering potential characterized by the electronic DOS behaviors and confirmed by HC and PSPS responses. Finally, we have looked at the response of HC and PSPS to the combined effects of perturbations to control the nontrivial behaviors above-reported. The results of this study provide a possible basis for the practical

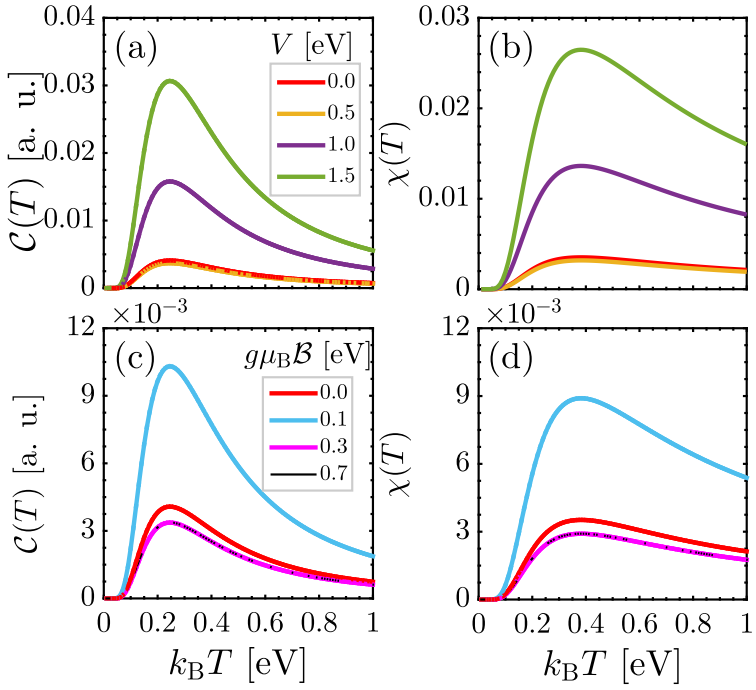

Fig. 7. Electric field- and Zeeman field-induced {(a),(c)} HC and {(b),(d)} PSPS of PbBiI compound at fixed scattering parameters $n_i = 10\%$ and $v_i = 0.5$ eV.

applications and control of information via the external perturbations in noncentrosymmetric QSHIs.

CRediT authorship contribution statement

Nguyen N. Hieu: Investigation, Formal analysis, Writing – review & editing. **Chuong V. Nguyen:** Software, Formal analysis, Writing – review & editing. **Huynh V. Phuc:** Software, Formal analysis, Writing – review & editing. **Bui D. Hoi:** Conceptualization, Investigation, Methodology, Formal analysis, Writing – review & editing. **Tran C. Phong:** Conceptualization, Investigation, Formal analysis, Writing – review & editing, Funding acquisition.

Declaration of competing interest

The authors declare that they have no known competing financial interests or personal relationships that could have appeared to influence the work reported in this paper.

Data availability

Data will be made available on request.

Acknowledgments

This research is funded by Vietnam National Foundation for Science and Technology Development (NAFOSTED) under grant number 103.01-2020.61.

References

[1] B. Yan, S.-C. Zhang, Rep. Progr. Phys. 75 (9) (2012) 096501.
[2] X.-L. Qi, S.-C. Zhang, Rev. Modern Phys. 83 (2011) 1057–1110.
[3] C.L. Kane, E.J. Mele, Phys. Rev. Lett. 95 (2005) 226801.
[4] M. Ezawa, New J. Phys. 14 (3) (2012) 033003.
[5] C.-C. Liu, W. Feng, Y. Yao, Phys. Rev. Lett. 107 (2011) 076802.
[6] C.-C. Liu, H. Jiang, Y. Yao, Phys. Rev. B 84 (2011) 195430.
[7] Y.-p. Wang, W.-x. Ji, C.-w. Zhang, P. Li, S.-f. Zhang, P.-j. Wang, S.-s. Li, S.-s. Yan, Appl. Phys. Lett. 110 (21) (2017) 213101.
[8] F. Reis, G. Li, L. Dudy, M. Bauernfeind, S. Glass, W. Hanke, R. Thomale, J. Schäfer, R. Claessen, Science 357 (6348) (2017) 287–290.
[9] X.-K. Hu, J.-K. Lyu, C.-W. Zhang, P.-J. Wang, W.-X. Ji, P. Li, Phys. Chem. Chem. Phys. 20 (2018) 13632–13636.
[10] Y. Ma, Y. Dai, L. Kou, T. Frauenheim, T. Heine, Nano Lett. 15 (2) (2015) 1083–1089.
[11] B.D. Hoi, M. Yarmohammadi, H.A. Kazzaz, J. Magn. Magn. Mater. 439 (2017) 203–212.
[12] M. Yarmohammadi, RSC Adv. 7 (2017) 10650–10659.
[13] S. Maekawa, S. Valenzuela, E. Saitoh, T. Kimura, Spin Current, in: Series on Semiconductor Science and Technology, OUP Oxford, 2012.
[14] M. Yarmohammadi, J. Magn. Magn. Mater. 417 (2016) 208–213.
[15] A. Manchon, H.C. Koo, J. Nitta, S.M. Frolov, R.A. Duine, Nature Mater. 14 (9) (2015) 871–882.
[16] D. Bercioux, P. Lucignano, Rep. Progr. Phys. 78 (10) (2015) 106001.
[17] M. Yarmohammadi, J. Magn. Magn. Mater. 426 (2017) 621–628.
[18] B.D. Hoi, M. Yarmohammadi, J. Magn. Magn. Mater. 451 (2018) 57–64.
[19] M. Yarmohammadi, Solid State Commun. 234–235 (2016) 14–20.
[20] M.Z. Hasan, C.L. Kane, Rev. Modern Phys. 82 (2010) 3045–3067.
[21] C. Mera Acosta, O. Babilonia, L. Abdalla, A. Fazzio, Phys. Rev. B 94 (2016) 041302.
[22] C. Mera Acosta, A. Fazzio, G.M. Dalpian, Npj Quantum Mater. 4 (1) (2019) 41.
[23] X.-k. Hu, Z.-x. Pang, C.-w. Zhang, P.-j. Wang, P. Li, W.-x. Ji, J. Mater. Chem. C 7 (2019) 9406–9412.
[24] S.-s. Li, W.-x. Ji, C.-w. Zhang, S.-j. Hu, P. Li, P.-j. Wang, B.-m. Zhang, C.-l. Cao, Sci. Rep. 6 (1) (2016) 23242.
[25] Y. Ma, L. Kou, A. Du, T. Heine, Nano Res. 8 (10) (2015) 3412–3420.
[26] Y. Sun, Y. Zhang, C. Felser, B. Yan, Phys. Rev. Lett. 117 (2016) 146403.
[27] H. Gao, W. Wu, T. Hu, A. Stroppa, X. Wang, B. Wang, F. Miao, W. Ren, Sci. Rep. 8 (1) (2018) 7436.
[28] I.A. Nechaev, S.V. Eremeev, E.E. Krasovskii, P.M. Echenique, E.V. Chulkov, Sci. Rep. 7 (1) (2017) 43666.
[29] J.-J. Zhou, W. Feng, C.-C. Liu, S. Guan, Y. Yao, Nano Lett. 14 (8) (2014) 4767–4771.
[30] H. Bui, M. Yarmohammadi, Physica E 103 (2018) 76–80.
[31] D.Q. Khoa, M. Davoudiniya, B.D. Hoi, M. Yarmohammadi, RSC Adv. 9 (2019) 19006–19015.
[32] M. Yarmohammadi, M.R. Ebrahimi, Phys. Rev. B 100 (2019) 165409.
[33] M. Yarmohammadi, Phys. Lett. A 380 (48) (2016) 4062–4069.
[34] P. Le, M. Yarmohammadi, J. Magn. Magn. Mater. 474 (2019) 137–143.
[35] M. Yarmohammadi, Phys. Rev. B 98 (2018) 155424.
[36] G. Mahan, Many-Particle Physics, in: Physics of Solids and Liquids, Springer US, 2000.
[37] G. Grosso, G. Parravicini, Solid State Physics, Elsevier Science, 2013.
[38] T.C. Phong, V.T. Lam, B.D. Hoi, J. Phys.: Condens. Matter 33 (32) (2021) 325502.
[39] C. Kittel, Introduction to Solid State Physics, Wiley, 2004.
[40] B.D. Hoi, L.V. Tung, P.T. Vinh, D.Q. Khoa, L. T. T. Phuong, Phys. Chem. Chem. Phys. 23 (2021) 2080–2087.